



HAL
open science

Wavelength-selective photoisomerisation of nitric oxide and nitrite in a rhodium complex

D. Schaniel, E.-E. Bendeif, T. Woike, H.-C. Böttcher, S. Pillet

► **To cite this version:**

D. Schaniel, E.-E. Bendeif, T. Woike, H.-C. Böttcher, S. Pillet. Wavelength-selective photoisomerisation of nitric oxide and nitrite in a rhodium complex. *CrystEngComm*, 2018, 20 (44), pp.7100 - 7108. 10.1039/C8CE01345D . hal-01926697

HAL Id: hal-01926697

<https://hal.univ-lorraine.fr/hal-01926697v1>

Submitted on 15 Mar 2022

HAL is a multi-disciplinary open access archive for the deposit and dissemination of scientific research documents, whether they are published or not. The documents may come from teaching and research institutions in France or abroad, or from public or private research centers.

L'archive ouverte pluridisciplinaire **HAL**, est destinée au dépôt et à la diffusion de documents scientifiques de niveau recherche, publiés ou non, émanant des établissements d'enseignement et de recherche français ou étrangers, des laboratoires publics ou privés.

Wavelength-selective photoisomerisation of nitric oxide and nitrite in a rhodium complex

D. Schaniel,^{*a} E.-E. Bendeif,^a T. Woike,^{a,b} H.-C. Böttcher,^c and S. Pillet^a

Photoinduced linkage isomers (PLIs) of NO and NO₂⁻ are selectively generated by a proper choice of irradiation wavelength at low temperature within the same molecular complex [Rh(NO)(NO₂)₂(Bu^tPH)₂]. The structures of the PLI are characterised by photocrystallography and the corresponding vibrational changes by infrared spectroscopy. Using red light about 37% of the κ ON isonitrosyl PLI can be produced while irradiation with blue light produces about 80% of the (O,O') chelating NO₂⁻ isomer. Upon heating the NO₂⁻ PLI undergoes several structural transformations, which are characterised by infrared spectroscopy.

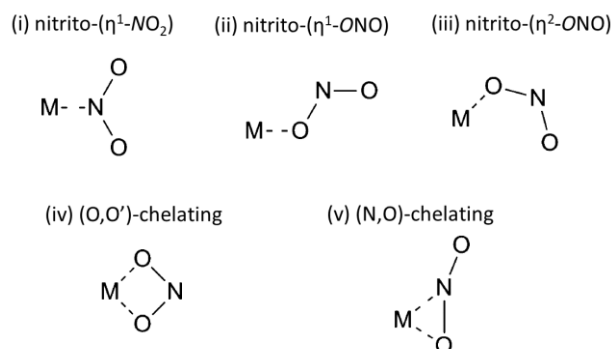
Introduction

The structural flexibility of the NO ligand in transition-metal complexes has been illustrated in many publications concerning photoinduced linkage isomers (PLI) [1-6]. Thereby the oxygen and nitrogen atom can adopt a variety of structural conformations (N-bound or O-bound) without the NO ligand being released. Some authors found indications that some of these PLI are implicated as precursor steps in the photorelease of NO [7]. PLI represents a rather strong modification of the molecular structure and hence we might expect significant influence of PLI on the structure and electronic properties of the whole molecule. However, most structural studies and DFT calculations show that the structural and electronic changes of the other ligands in the molecule are rather small [4], such that in good approximation the NO ligand can be treated in a partial M-NO description such as the Enemark-Feltham scheme {MNO}ⁿ, with n the total number of electrons associated with the metal d and π^* (NO) orbitals [8]. This description is based on the donor-acceptor properties within MNO and especially the backbonding of the metal to the NO via the π^* (NO). In this description the complex [Rh(NO)(NO₂)₂(Bu^tPH)₂] has a {RhNO}⁸ configuration, for example, formally Rh(d⁸)NO⁺. However, in view of the observed structural parameters of [Rh(NO)(NO₂)₂(Bu^tPH)₂] with the NO being formally a bent NO⁻ ligand, what is clearly indicated by the Rh-N-O angle of 125° in the ground state, the formal oxidation state of Rh should be discussed as Rh(III). If more than one photoswitchable ligand with the ability to form PLI is present, the situation gets more complicated and we might expect a more intricate interplay between the electron density distribution and the PLI properties. Also in this case, the simple correlation between the positive or negative shift of vibrational frequencies, e.g. of ν (NO), and the nature of the PLI [9,10] is no longer valid. We need to get a thorough crystallographic description of the

structure in order to safely interpret the changes in the vibrational spectra [11-13]. In the present case the two photoswitchable ligands NO and NO₂⁻ dispose of a plethora of potential PLI. Especially NO₂⁻ with its increased degrees of freedom offers many different PLI as shown in Scheme 1 (see e.g. Ref. [12]).

Scheme 1: Five main PLI for NO₂⁻.

Some of these geometries were already characterised by photocrystallography in compounds with different central atoms [13,14]. Evidence for multiple PLI within one complex was given by Kovalevsky et al. [14] for the hexacoordinated



ruthenium complex [Ru(NO)(NO₂)(bpy)₂](PF₆). From Fourier difference maps the photoswitched ligands can be identified as a function of irradiation wavelength and temperature.

We present a combined photocrystallographic and infrared spectroscopic study of PLI in [Rh(NO)(NO₂)₂(Bu^tPH)₂]. We show that irradiation in the red spectral range generates the isonitrosyl configuration of the NO ligand while irradiation in the blue spectral range generates the (O,O')-chelating configuration of the NO₂⁻ ligand. Both PLI influence the vibrations of the other photoswitchable ligand, such that an unambiguous PLI identification is only possible by photocrystallography. Long-time irradiation in the blue spectral range further leads to NO photorelease, which again can be quantified by photocrystallography.

Experimental

^a Université de Lorraine, CNRS, CRM2, F-54000 Nancy, France.

^b Institut für Festkörper- und Materialphysik, TU Dresden, Zellescher Weg 16, Dresden, Germany.

^c Departement Chemie der Ludwig-Maximilians-Universität, Butenandtstraße 5-13, 81377 Munich, Germany.

† Electronic address: Dominik.schaniel@univ-lorraine.fr.

Synthesis and preparation of $[\text{Rh}(\text{NO})(\text{NO}_2)_2(\text{Bu}_2\text{PH})_2]$ was performed according to the procedure described in Ref. [15].

Infrared spectroscopy

Infrared spectra were collected on a Nicolet 5700 FTIR spectrometer in the range $4000\text{--}360\text{ cm}^{-1}$ with a resolution of 2 cm^{-1} . The sample was mixed with KBr (spectroscopy grade), finely ground, and pressed to pellets. The pellets were glued with silver paste to a copper sample holder on the cold finger of an Oxford Optistat V01, allowing temperature regulation in the range $9\text{--}300\text{ K}$. KBr windows allow for in-situ irradiation of the sample in the ultraviolet, visible and near infrared spectral range.

Photocrystallography

Single-crystal X-ray diffraction data were collected on a SuperNova Microfocus diffractometer equipped with a two-dimensional ATLAS detector, using $\text{Mo K}\alpha$ radiation ($\lambda = 0.71073\text{ \AA}$) and a Helijet He open-flow cryosystem. The temperature was fixed at 10 K . A single crystal was mounted on a glass fiber using vacuum grease. Diffraction data were first collected at 10 K in the ground state (GS) using ω scans. The unit-cell determination and data reduction were performed using the *CrysAlisPRO* program suite [16] on the full data set. 22314 reflections were measured up to a maximum resolution of $\sin(\theta)/\lambda = 0.76\text{ \AA}^{-1}$ and merged to 4104 unique reflections ($R_{\text{int}} = 0.0452$). A numerical absorption correction was performed according to the crystal faces of the $[\text{Rh}(\text{NO})(\text{NO}_2)_2(\text{Bu}_2\text{PH})_2]$ crystal. The corresponding crystal structure was solved in the space group *Pbca* by direct methods with SHELXS software and refined on F^2 by weighted full matrix least-squares methods using the *SHELXL* program [17]. All non-H atoms were refined anisotropically. H atoms were located in difference Fourier maps and treated using a riding model, constraining the isotropic displacement parameters to $1.2U_{\text{eq}}$ of the parent C atom. The crystal structure of $[\text{Rh}(\text{NO})(\text{NO}_2)_2(\text{Bu}_2\text{PH})_2]$ exhibits strong disorder which was taken into account using 2 positions for the phosphorus atoms of the di-*tert*-butylphosphine ligands (labelled P and P') with approximately 78% and 22% occupancies, and several configurations for the *tert*-butyl moieties. The Rh atom is furthermore disordered symmetrically around the position (0.5, 0.5, 0.5) (distance to the special position is approximately 0.29 \AA) generating the crystallographic center of inversion in the *Pbca* space group. The nitrosyl ligand (N1-O1) is disordered about the center of inversion. Releasing all the symmetry constraints and refining the structure in space group *P1* did not allow resolving the disorder. Figure 1 shows the complex and the disorder over the two positions (small ball-stick model for the second position). We note that the NO_2^- ligand is not disordered.

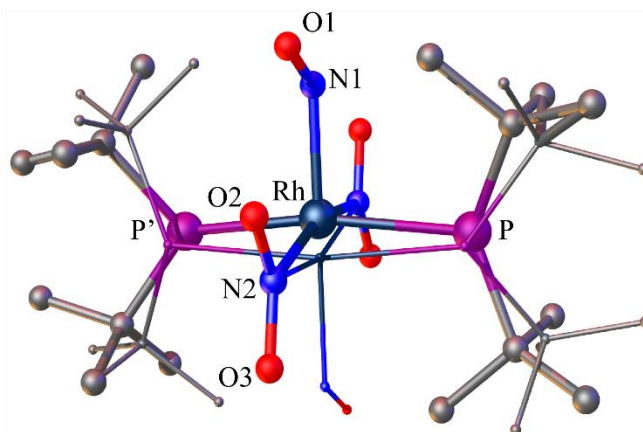


Figure 1: Ball and stick representation of the structure of $[\text{Rh}(\text{NO})(\text{NO}_2)_2(\text{Bu}_2\text{PH})_2]$ in the ground state. The two differently sized balls represent the two positions over which the molecule is disordered.

The sample was then irradiated at 10 K with a diode laser of 635 nm ($P = 60\text{ mW}$) for 20 min in the dark, until the photo-stationary state was reached. Complete diffraction data were collected in the photo-stationary state; no space-group change occurs with respect to the ground state (space group *Pbca*). The unit-cell parameters change only slightly from $a = 12.1515(6)\text{ \AA}$, $b = 12.5518(5)\text{ \AA}$ and $c = 15.2014(7)\text{ \AA}$ in the GS to $a = 12.1855(7)\text{ \AA}$, $b = 12.5477(6)\text{ \AA}$ and $c = 15.1668(8)\text{ \AA}$ in the 635 nm photo-induced state. 20199 reflections were measured up to a maximum resolution of $\sin(\theta)/\lambda = 0.76\text{ \AA}^{-1}$, and merged to 4056 unique reflections ($R_{\text{int}} = 0.0447$). Empirical absorption correction was performed. All data are given in Table 1.

Photo-difference maps were calculated for visualization of the light-induced changes in electron density, and for identification of the related structural changes from the GS to the 635 nm photoinduced state. Common independent reflections between the GS and photo-irradiated state were used to compute the experimental X-ray photo-difference map by Fourier transform of the difference $[F_{\text{photo-irradiated}}^{\text{obs}}(hkl) - F_{\text{GS}}^{\text{obs}}(hkl)]$, using the structure factor phases from the GS structural refinement. 3955 common independent reflections were included in the calculation. The photodifference map is shown in Figure 2.

In a second step, after having relaxed the PLI created by 635 nm by heating to room temperature, the same sample was irradiated at 10 K with a diode laser of 445 nm ($P = 120\text{ mW}$) for 20 min in the dark. Complete diffraction data were collected in the photo-stationary state; no space-group change occurs with respect to the ground state (space group *Pbca*). The unit cell parameters changed to $a = 12.2256(15)\text{ \AA}$, $b = 12.5161(11)\text{ \AA}$ and $c = 15.2656(15)\text{ \AA}$ in the 445 nm photo-induced state. 21397 reflections were measured up to a maximum resolution of $\sin(\theta)/\lambda = 0.76\text{ \AA}^{-1}$, and merged to 4107 unique reflections ($R_{\text{int}} = 0.1063$). Numerical absorption correction was performed. Photodifference maps were calculated from these data as shown in Figure 4. These data are of lower quality than the

ground state and the 635 nm photoirradiated state, as highlighted by the high internal agreement factor R_{int} .

Table 1: Crystallographic data and refinement details for $[\text{Rh}(\text{NO})(\text{NO}_2)_2(\text{Bu}^i_2\text{PH})_2]$ in the ground and photo-irradiated states.

	Ground state	Photo-irradiated state 635nm	Photo-irradiated state 445nm
Crystal data			
Chemical formula	$\text{RhN}_3\text{O}_5\text{P}_2\text{C}_{16}\text{H}_3$ 8	$\text{RhN}_3\text{O}_5\text{P}_2\text{C}_{16}\text{H}_3$ 8	$\text{RhN}_3\text{O}_5\text{P}_2\text{C}_{16}\text{H}_3$ 8
M_r (g.mol ⁻¹)	517.34	517.34	517.34
Crystal system, space group	orthorhombic, <i>Pbca</i>	orthorhombic, <i>Pbca</i>	orthorhombic, <i>Pbca</i>
Z	4	4	4
<i>a</i> (Å)	12.1515(6)	12.1855(7)	12.2256(15)
<i>b</i> (Å)	12.5518(5)	12.5477(6)	12.5161(11)
<i>c</i> (Å)	15.2014(7)	15.1668(8)	15.2656(15)
α (°)	90	90	90
β (°)	90	90	90
γ (°)	90	90	90
<i>V</i> (Å ³)	2318.5(2)	2319.0(2)	2335.9(4)
ρ_{calc} (g cm ⁻³)	1.482	1.482	1.470
μ (mm ⁻¹)	0.904	0.903	0.897
Crystal size (mm)	0.18 x 0.25 x 0.33	0.18 x 0.25 x 0.33	0.18 x 0.25 x 0.33
Data collection			
Temperature (K)	10	10	10
No. of measured reflections	22314	20199	21397
θ range (°)	3.161-32.955	3.164-32.943	3.146-32.884
No. of independent reflections, R_{int}	4104, 0.0452	4056, 0.0447	4107, 0.1063
No. of observed reflections [$I > 2\sigma(I)$]	3216	3142	2024
Refinement			
No. of parameters	214	157	221
^a R_1 [$F^2 > 2\sigma(F^2)$]	0.0759 [0.0552]	0.0811 [0.0606]	0.1570 [0.0798]
^b wR_2 [$F^2 > 2\sigma(F^2)$]	0.1525 [0.1357]	0.1646 [0.1501]	0.2311 [0.1812]
^c GoF	1.049	1.268	0.983
$\Delta\rho_{max}, \Delta\rho_{min}$ (eÅ ⁻³)	1.542, -0.937	1.312, -0.829	1.486, -0.798

$$^a R_1 = \sum |F_o - F_c| / F_o, \quad ^b wR_2 = \{ \sum [w(F_o^2 - F_c^2)^2] / \sum [w(F_o^2)^2] \}^{1/2}, \quad ^c GoF = \{ \sum [w(F_o^2 - F_c^2)^2] / (N_{obs} - N_{var}) \}^{1/2}.$$

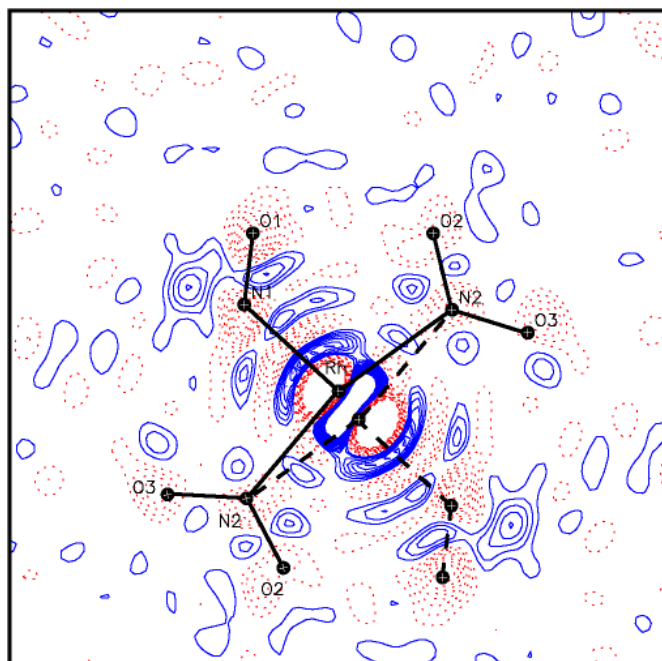


Figure 2: Section of the 635nm photo-difference map in the RhN1N2 plane with isocontour of $\pm 0.2 \text{ e}\text{\AA}^{-3}$ (red-negative and blue positive electron density).

Results

Photocrystallography

The 635 nm photo-difference map (Figure 2) shows important structural changes between the ground state (GS) and the photo-irradiated state. A strong contribution occurs in the vicinity of Rh, with negative difference electron density at the Rh position in GS, and positive contribution on the center of inversion. This is most probably related to a displacement of the Rh atom in the photo-irradiated state into the direction of the center of inversion at (0.5, 0.5, 0.5). The two nitrosyl (NO) and nitrito (NO_2) ligands exhibit very different characteristics. Strong negative contributions at the N1 and O1 positions together with positive contributions indicate a reorientation of the nitrosyl ligand. On the contrary, no significant features can be detected in the neighborhood of the nitrito ligand. The photo-difference map therefore evidences a selective photo-isomerisation process of the nitrosyl ligand being triggered by the 635 nm excitation.

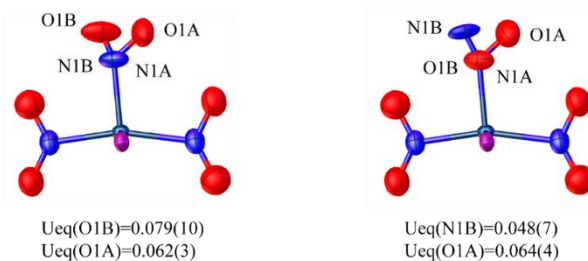


Figure 3: Comparison of the two refined structural models considering a nitrosyl (left) and isonitrosyl (right) coordination mode for the 635 nm photoirradiated state.

According to the observations derived from the $\lambda = 635\text{nm}$ photo-difference map, a structural model of the photo-irradiated state was defined and refined against the experimental diffraction data. All the atoms, except N1 and O1 were considered as in the ground state configuration, and refined as a rigid group. Two configurations were considered for the nitrosyl ligand, one nitrosyl configuration (N1A- O1A) corresponding to the ground state with GS population P_{GS} , and one nitrosyl configuration (N1B-O1B) corresponding to the photo-irradiated state detected in the photodifference map with population $P_{PI}=1-P_{GS}$. The refinement converged to a refined population of the photo-irradiated state of $P_{PI}=0.35(2)$. In order to define whether the coordination mode in the photo-irradiated state is a nitrosyl (Rh-N1B-O1B) or an isonitrosyl (Rh-O1B- N1B) configuration, the two possibilities were separately refined. The results of the two refinements are given in Figure 3. The corresponding refinement agreement statistics are very similar for the two structural models (marginally better for the nitrosyl hypothesis), and therefore do not allow a decisive choice to be made. One can further inspect the thermal ellipsoids of the terminal O1B and N1B atoms. In the nitrosyl configuration, the equivalent atomic displacement parameter (ADP, Ueq) for O1B is higher than the ADP of O1A in the ground state. On the contrary, in the isonitrosyl configuration, the ADP of N1B is clearly too small ($0.048(7) \text{ \AA}^2$) with respect to O1A in the ground state. This comparison is very informative, but does not allow clearly discriminating between the nitrosyl or isonitrosyl hypotheses. The refined positions of N1B-O1B indicate a strong increase of the Rh-N1-O1 angle from $125.3(1)^\circ$ in the ground state to $160.7(10)^\circ$ in the 635nm photoirradiated state.

The 445 nm photodifference map shown in Figure 4 evidences very different features by comparison with the 635 nm photodifference map (Figure 2). At first, negative difference densities are detected at the positions of O1 and N1, but without any positive contributions which would have been the signature of a photoinduced metastable state of the N1-O1 ligand as detected with 635 nm irradiation. This could be rather attributed to NO release induced by the 445 nm irradiation. Negative contributions are also observed at the N2, O2 and O3 positions, with three positive peaks, evidencing a photoisomerisation of the nitrito ligand. The three positive peaks could correspond to a configuration with Rh coordinated to both O2 and O3, the binding mode to Rh is therefore modified by 445 nm irradiation. This hypothesis, corresponding to the (O,O')-chelating configuration of the NO_2^- ligand, is depicted as green dotted lines in Figure 4. According to these observations, a structural model was built with a fraction of the nitrito ligand switched to the putative orientation. The switched nitrito O2-N2-O3 ligand was refined as a rigid group with N2-O2 and N2-O3 distances, and O2-N2-O3 angle equal to the ground state values. The refinement converged reasonably, allowing for picturing some trends. The refined fraction of the photo-irradiated state is $P_{PI} = 0.39(2)$, which is even higher than the value obtained for the 635 nm photo-irradiated state. In the ground state, the Rh atom is connected to the N2 atom with a

Rh-N2 bond distance of $2.065(3)\text{\AA}$, while in the photo-induced state, the Rh-O bond distances are Rh-O2B = $2.18(2)\text{\AA}$, and Rh-O3B = $2.29(3)\text{\AA}$.

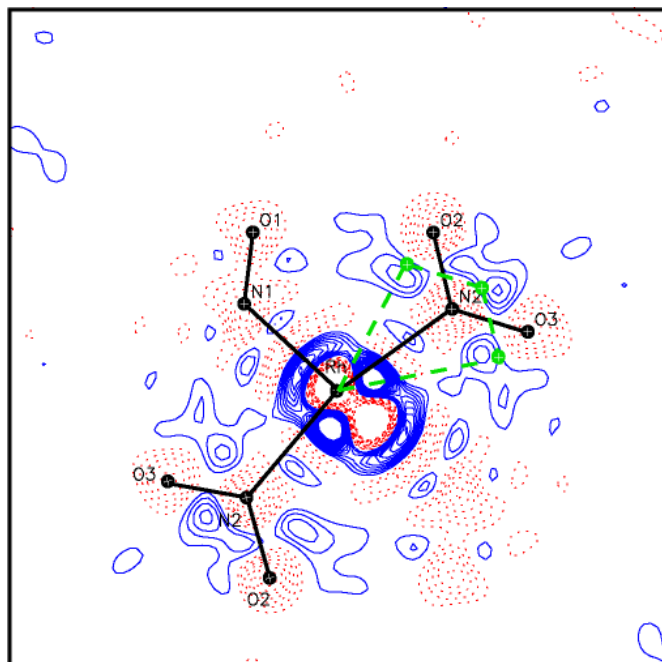


Figure 4: Section of the 445nm photo-difference map in the RhN1N2 plane with isocontour of $\pm 0.2 \text{ e\AA}^{-3}$ (red-negative and blue positive electron density).

In order to estimate the amount of NO release, evidenced by the photocrystallographic results, we have performed the same structural refinement as before, while varying the population of the nitrosyl ligand from 100 % to 40 % (varying the occupancy of the N1 and O1 atoms in the structural refinement). Since the atomic displacement parameters are strongly correlated to the occupancy factors in a structural refinement, decreasing the N1 and O1 occupancies result in decreased refined atomic displacement parameters. The results of the refinements are illustrated in Figure 5. As expected, as the fraction of NO release increases (and conversely the occupancy factors of O1 and N1 decrease in the refinement), the refined equivalent atomic displacement parameters decrease. At nearly 50 % NO release, the obtained values are similar to the ground state values. This is obviously a rough estimate, but we can nevertheless conclude

that 445 nm irradiation induces a high contribution of NO release. Note that the NO release and the correspondingly reduced crystal quality explain the higher internal agreement factor R_{int} for the 445nm irradiation compared to those obtained for GS and the irradiation with 635nm.

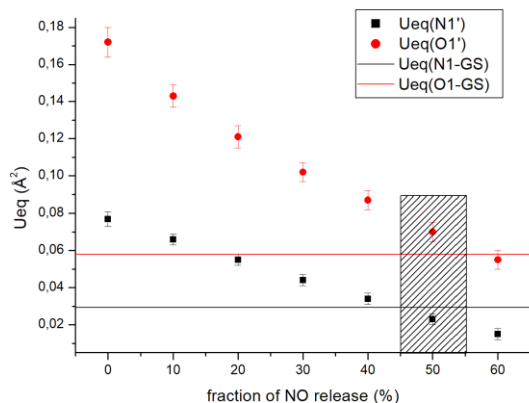


Figure 5: Evolution of the refined equivalent atomic displacement parameter U_{eq} for O1 and N1 as a function of the fixed fraction of NO release (the fraction of NO release is directly related to the occupancy factors of N1 and O1 in the structural refinement).

Infrared spectroscopy

Comparing the proposed structural changes based on the analysis of the photodifference maps to the infrared spectra, measured at 10K, one should be able to identify the corresponding decrease of the GS bands and assign the novel bands after photoirradiation to the different PLI. Inspecting first the changes in the NO stretching vibration $\nu(\text{NO})$, we find that irradiation with 635 nm reduces the GS band at 1687 cm^{-1} by 37 % (Figure 6). A new band at 1781 cm^{-1} with a shoulder at 1768 cm^{-1} arises as well as a weaker band at 1865 cm^{-1} . In terms of frequency shift, this amounts to a positive shift of 94 and 178 cm^{-1} . The area of these new bands is considerably smaller than that of the GS. If we assign the $\delta(\text{Rh-N-O})$ deformation mode to the GS band at 565 cm^{-1} , we find the corresponding new band at 587 cm^{-1} , i.e., a shift to higher energies by 22 cm^{-1} . The $\nu(\text{Rh-N})$ band is at 445 cm^{-1} in GS and decreases upon irradiation, however the corresponding new band could not be unambiguously identified. Below 400 cm^{-1} the signal-to-noise ratio becomes unfavourable so that weak bands arising in this region might not be detected. In this low-frequency region, we tentatively assign also the wagging mode of NO_2^- , $\rho(\text{NO}_2)$, at 597 cm^{-1} . It decreases upon irradiation and a new band is arising at 610 cm^{-1} , i.e. a shift to higher wavenumbers by 13 cm^{-1} . The assignment of the 565 and 597 cm^{-1} bands to $\delta(\text{Rh-N-O})$ and $\rho(\text{NO}_2)$ is not unambiguous, but based on available literature [18,19], we assign the higher energetic band to the wagging mode. Looking now to the other spectral ranges of the NO_2^- vibrations, we observe reductions of the band-intensities at 1388 cm^{-1} ($\nu_{as}(\text{N=O}_2)$) and 1308 cm^{-1} ($\nu_s(\text{N-O}_2)$), without the appearance of clearly distinguishable new bands. Taking into account the overlap with neighboring bands, the reduction of the area of the central band at 1388 cm^{-1} necessarily induces a

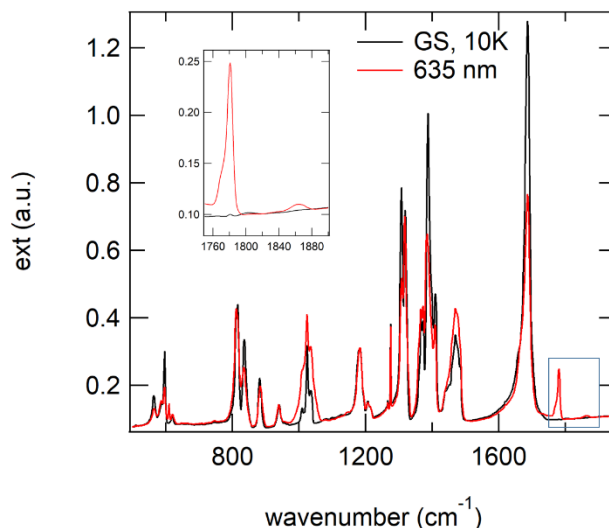


Figure 6: Infrared spectra of GS (black line) and after irradiation with 635 nm (red line) at 10 K. The insert shows a zoom onto the region $1750\text{-}1900 \text{ cm}^{-1}$.

reduction of the band amplitude of neighboring bands. This is actually the case for the band at 1408 cm^{-1} . For the doublet at $1373/1366 \text{ cm}^{-1}$ on the other hand we observe an increase in amplitude. Moreover, the main band at 1388 cm^{-1} exhibits after irradiation three maxima at 1389 , 1386 , and 1382 cm^{-1} , with the main maximum at 1382 cm^{-1} shifted by -6 cm^{-1} with respect to GS. One may thus conclude that the new band $\nu^*_{as}(\text{NO}_2)$ is shifted by about -6 cm^{-1} to 1382 cm^{-1} . Similar reasoning can be applied to the $\nu_s(\text{N-O}_2)$ band at 1308 cm^{-1} . The area of this band is significantly reduced, while the intensity of the immediate and strongly overlapping neighboring band at 1319 cm^{-1} is hardly affected. Moreover, a shoulder at 1325 cm^{-1} appears after irradiation. Hence we conclude that the new $\nu^*_s(\text{N-O}_2)$ band is shifted to slightly higher energies (around 1315 cm^{-1}). The deformation mode $\delta(\text{NO}_2)$ of the GS is found at 836 cm^{-1} overlapping with the bands at $817/813 \text{ cm}^{-1}$. After irradiation the absorption between the two bands increases indicating the generation of a new band around 826 cm^{-1} , corresponding to a shift of -10 cm^{-1} to lower energies.

Irradiation with blue light ($\lambda = 445 \text{ nm}$) leads to much more pronounced changes in the vibrational spectrum (see Figure 7). The area of the $\nu(\text{NO})$ vibration at 1687 cm^{-1} is reduced by more than 80 %. The remainder exhibits a double peak at 1686 and 1671 cm^{-1} . New peaks with significantly smaller area arise at 1746 , 1775 , and 1859 cm^{-1} . Like in the case of 635 nm irradiation these bands are shifted to higher energies with respect to GS, however, they appear at different wavenumbers. Equally the areas of the $\delta(\text{Rh-N-O})$ deformation mode and the $\nu(\text{Rh-N})$ stretching mode at 565 cm^{-1} and 445 cm^{-1} decrease by more than 80 %. Since the band at 588 cm^{-1} increases we assign this band to the new $\delta^*(\text{Rh-N-O})$ vibration. Again the new $\nu^*(\text{Rh-N})$ band cannot be unambiguously identified in the spectrum. The NO_2^- related vibrations are also changed significantly. The wagging mode $\rho(\text{NO}_2)$ shifts from 597 cm^{-1} to 622 cm^{-1} , superposed to an original GS band at this wavenumber. The $\nu_{as}(\text{N=O}_2)$ band at 1388 cm^{-1} is no longer visible. Three new

bands at 1391, 1385, and 1380 cm^{-1} arise. The double band of GS at 1373/1367 cm^{-1} transforms into a single band at 1371 cm^{-1} with two shoulders at 1365 cm^{-1} and 1358 cm^{-1} . We infer that the $\nu_{\text{as}}(\text{N}=\text{O}_2)$ band does not simply shift but splits into several components corresponding to the new $\nu_{\text{as}}^*(\text{N}=\text{O}_2)$ band. The symmetric stretching vibration $\nu_{\text{s}}(\text{N}=\text{O}_2)$ also vanishes almost completely. The area of the neighboring band at 1319 cm^{-1} is in consequence reduced also, but exhibits now a shoulder at about 1326 cm^{-1} , which might be assigned to the new $\nu_{\text{s}}^*(\text{N}=\text{O}_2)$. The deformation mode $\delta(\text{NO}_2)$ of the GS at 836 cm^{-1} is strongly modified. A shoulder at 845 cm^{-1} appears and a new maximum is formed at 828 cm^{-1} , whereas the area of the new bands is smaller than that of the GS. The neighboring doublet at 817/813 cm^{-1} is also modified, the new band exhibiting a maximum at 811 cm^{-1} with shoulders at 795 cm^{-1} and 820 cm^{-1} .

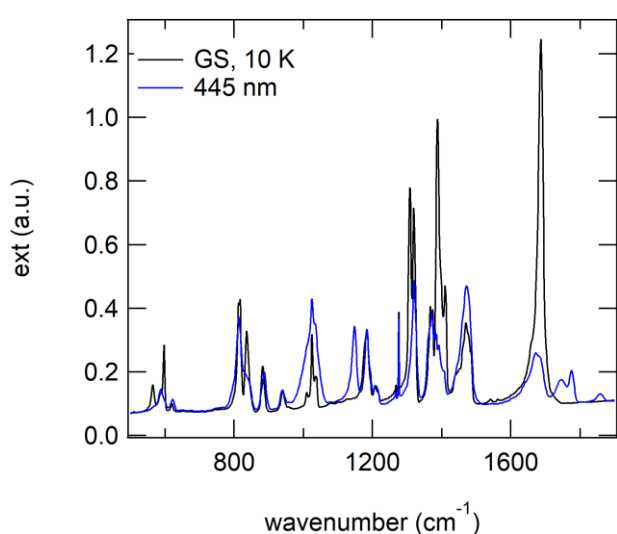


Figure 7. Infrared spectra of GS (black line) and after irradiation with 445 nm (blue line) at 10 K.

Additionally, a strong new band arises at 1148 cm^{-1} . This band most probably corresponds to the $\nu(\text{N}-\text{O})$ stretching vibration of the (O,O')-chelating PLI (O=N-O). The corresponding $\nu(\text{N}=\text{O})$ mode cannot be unambiguously detected, probably it is found around 1470 cm^{-1} , since this band increases upon irradiation. This interpretation is in accordance with the assignment of the two stretching vibrations in $[\text{Re}(\text{dmb})(\text{CO})_3(\text{ONO})]$ based on ^{15}N isotope substitution [20] as well as studies on a $[\text{Cu}(\text{CH}_3\text{CN})_4(\text{NO}_2)_2](\text{PF}_6)_2$ complex [21] and a thermally induced nitro-nitrito(O,O) isomerisation in a nickel complex [22]. Photoexcitation as a function of wavelength reveals that this $\nu(\text{N}-\text{O})$ band at 1148 cm^{-1} arises by irradiation with 532 nm, has a maximum upon irradiation with 445 nm, and is less pronounced again upon irradiation with 405 nm. This wavelength dependence is reflected also in the behaviour of the $\nu(\text{P}-\text{H})$ band. Since the hydrogen atoms are only indirectly influenced by the structural rearrangement of the NO and NO_2^- ligands, the modification of the $\nu(\text{P}-\text{H})$ is due to the overall change of the electron density distribution. Upon irradiation the GS band at 2351 cm^{-1} is shifted to lower wavenumbers: 2348

cm^{-1} for irradiation with 635 nm, 2340 cm^{-1} for irradiation with 445 nm, 2341 cm^{-1} for irradiation with 405 nm (see Fig. S1 of supplementary material).

Upon heating, the PLI decays via intermediate states back to the GS. Figure 8 illustrates this behaviour for the case of irradiation with 445 nm at $T = 10$ K, for selected temperatures in the range 10 – 280 K at which significant changes occur. For full temperature dependence see supplementary material (Figures S2-S6).

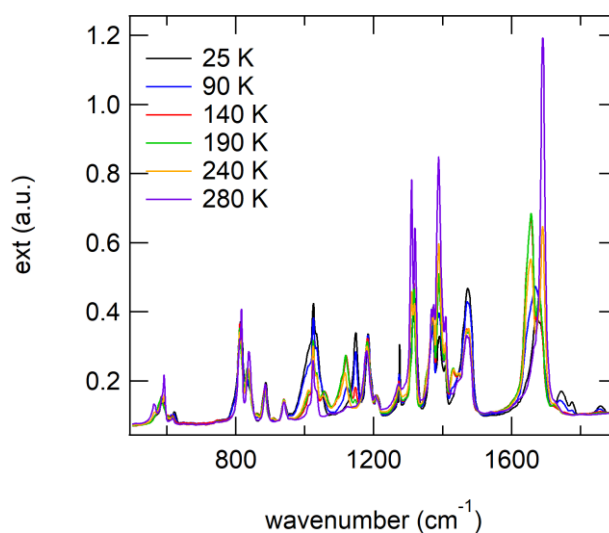


Figure 8. Infrared spectra upon heating after irradiation with 445 nm at 10 K.

The two bands at 1865 cm^{-1} and 1775 cm^{-1} relax upon heating to 130 K, but starting from around 80 K a new band arises at 1657 cm^{-1} , thus -30 cm^{-1} shifted with respect to the GS $\nu(\text{NO})$ band at 1687 cm^{-1} . This band at 1657 cm^{-1} remains up to about 240 K, where it starts to relax back to the GS band. The NO_2^- related vibrational bands evolve also upon heating. Up to about 80 K new broad bands arise at 1425/1408/1384/1350 cm^{-1} , which evolve back to GS upon heating above 240 K. Equally, the $\nu_{\text{s}}(\text{NO}_2)$ band builds out a peak at 1316 cm^{-1} around 80 K, which at about 240 K shifts back to the GS position at 1308 cm^{-1} . A similar temperature evolution is observed for the $\delta(\text{NO}_2)$ mode at 836 cm^{-1} . Around 80 K new bands arise at 833 and 813 cm^{-1} , which evolve back to the GS positions at 836 cm^{-1} and 817/813 cm^{-1} upon heating to 240 K. The band at 1148 cm^{-1} shows a particularly interesting evolution. Around 80 K a band at 1121 cm^{-1} becomes clearly visible at the expense of the 1148 cm^{-1} band. Until 140 K this band grows and develops a shoulder at 1105 cm^{-1} and an additional band at 1056 cm^{-1} . These bands stay unchanged until about 240 K where they start to decrease and the GS is re-established. We can only speculate on the nature of this intermediate PLI. In the literature there is a report on a transient species in $[\text{Co}(\text{NH}_3)_5(\text{NO}_2)]\text{Cl}_2$ [19], where a broad band around 1100 cm^{-1} was tentatively assigned to the $\nu(\text{N}-\text{O})$ vibration of a chelating (N,O) configuration.

Interestingly the band at 1657 cm^{-1} as well as two bands at 1108 and 1127 cm^{-1} arise also upon heating after irradiation with red light (635 nm). These bands develop starting from 80 K to about

130 K, temperature where the corresponding PLI has completely relaxed, and then decrease upon heating to 260 K. Figure 9 illustrates the main evolutions, for a complete temperature dependence see Figures S7 and S8 of the supplementary material.

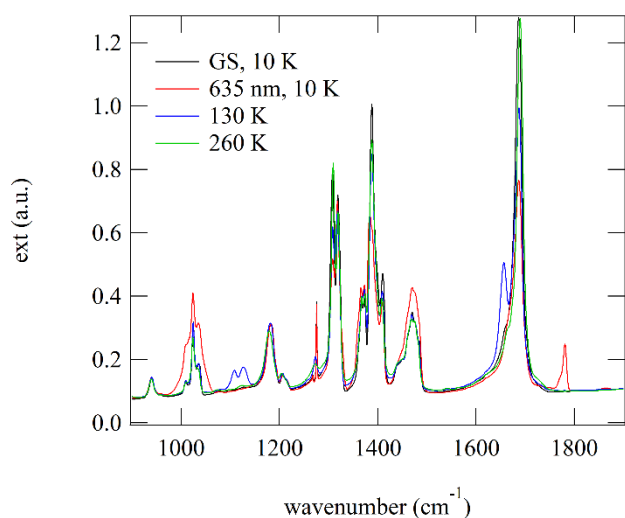


Figure 9. Infrared spectra upon heating after irradiation with 635 nm at 10 K.

These measurements indicate that the relaxation of both PLI, the one generated with red and the one generated with blue light, occur via intermediated steps, probably further isomeric structures. Moreover, they exhibit a similar infrared signature. In order to shine more light on this behaviour we performed irradiations with blue and red light at 100 K, temperature at which the relaxation of the different PLI has set in. Figure 10 shows the results. Indeed, we observe that at 100 K we find the same signature for both irradiation wavelengths and corresponding to that obtained during heating after irradiation at 10 K. This is a strong indication that both PLI have a similar relaxation channel.

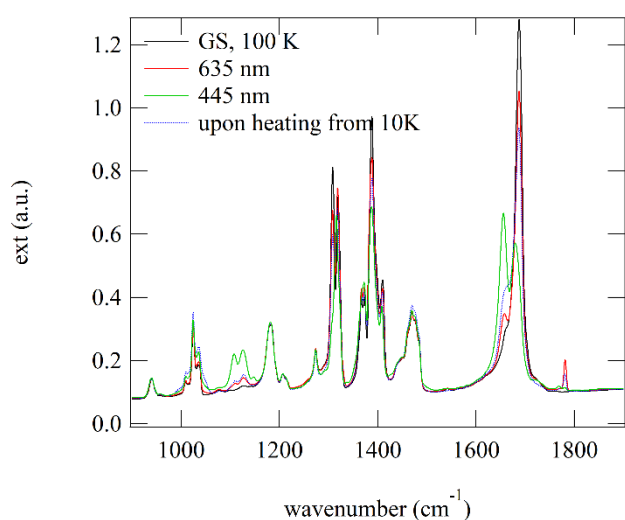


Figure 10. Comparison of infrared spectra obtained after irradiation at 100 K with blue (445 nm) and red (635 nm) light, and corresponding spectrum obtained during heating after irradiation with red light at 10 K.

Discussion

For the interpretation of the PLI structures we can rely on the combined photocrystallographic and infrared spectroscopic measurements. We note at first, that in the case of 635 nm irradiation the $\nu(\text{NO})$ vibration shifts to higher energies. This is analogous to observations in octahedrally coordinated $\{\text{PtNO}\}^8$ complexes [10], where the red light irradiation led to a shift to higher wavenumbers. In these cases, DFT calculations showed that the PLI corresponds to an isonitrosyl (κON) configuration of NO, whereby the NO flips over to a Pt-O-N with a slightly larger angle (127°) compared to the GS Pt-N-O (118°) and a significantly longer Pt-O bond length of 2.72 \AA compared to 2.18 \AA in the GS configuration Pt-N-O. We suppose that in the RhNO complex we encounter the same situation. The photocrystallographic measurements show that the angle is increased from 125° to 161° . While these crystallographic measurements do not allow an unambiguous identification of an isonitrosyl configuration, since the analysis based on the ADPs is not conclusive, the analogy to the PtNO compounds together with the infrared results leads us to the hypothesis that this observed PLI corresponds to an isonitrosyl configuration Rh-O-N, which is also consistent with a decay temperature of about 130 K. Having said that, we might put forward a second hypothesis. The increase of the ADP parameters when refining a nitrosyl (N-bound) configuration points to an overestimation of the actual electron density present on the NO ligand. In other words, the NO might evolve from (formally) NO^- in the GS towards NO^+ in the PLI. Accordingly, the oxidation state of the rhodium would have changed from Rh(III) in the GS to Rh(I) in the PLI. The observed higher $\nu(\text{NO})$ vibration energy would be compatible with the NO^+ assignment. Note however, that the Rh(I) oxidation state is very rare for five-fold coordinated complexes, it occurs in general in four-fold coordination in square-planar configuration.

The irradiation with red light seems to affect the NO_2^- ligands only slightly, given the minor changes in the photodifference maps. The observed changes in the infrared spectra suggest that a small population of a nitrite isomer is present, however it is too small to be analysed by photocrystallography.

The structural changes induced by blue light irradiation show a clear PLI of the NO_2^- ligand. The photodifference maps indicate an (O,O')-chelating configuration, which could be refined satisfactorily. With this chelating nitrite ligand, the complex has evolved from a fivefold to a sixfold coordination, and hence the electron density distribution is significantly altered. These changes are responsible for the observed shifts of the $\nu(\text{NO})$ vibrations in this case, again to higher wavenumbers. Further, the band areas are significantly smaller than in the GS, indicating a reduced dipole moment in the PLI state, making it difficult to clearly identify the various new bands, which sometimes overlap with GS bands, e.g. for the $\rho^*(\text{NO}_2)$ and $\delta^*(\text{Rh-N-O})$ bands. A notable exception is the rather intense band at 1148 cm^{-1} , which we assign to the $\nu(\text{N-O})$ vibration of the chelating (O,O')-configuration. The corresponding $\nu(\text{N=O})$ vibration at 1470 cm^{-1} is again overlapping with a GS band and

therefore deduced indirectly by the intensity change of this band.

Finally, we note, that long-time irradiation with blue light leads to significant NO release, as shown by photocrystallography. Corresponding infrared measurements as a function of irradiation fluence $Q = I \cdot t$ confirm this, as can be seen by the appearance of a band at 2220 cm^{-1} , corresponding to free NO in KBr, for irradiations beyond $Q = 200 \text{ J/cm}^2$ (see Figure S9 in the supplementary material).

The particularity of the $[\text{Rh}(\text{NO})(\text{NO}_2)_2(\text{Bu}^t_2\text{PH})_2]$ complex is that it offers the possibility to induce both, PLI of NO and of NO_2^- , by using different wavelengths. This indicates a certain flexibility of the rhodium metal to accommodate the corresponding electron density changes. This is much less observed in hexacoordinated ruthenium nitro-nitrosyl compounds, where up to now only the $[\text{Ru}(\text{NO})(\text{NO}_2)(\text{bpy})_2](\text{PF}_6)$ showed this capacity, while other compounds such as $[\text{Ru}(\text{NO})(\text{NO}_2)_2(\text{OH})\text{L}_2]$ ($\text{L} = \text{pyridine}$ or $\text{pyridine-derivatives}$), $\text{K}_2[\text{Ru}(\text{OH})(\text{NO})(\text{NO}_2)_4]$, $\text{Na}_2[\text{Ru}(\text{OH})(\text{NO})(\text{NO}_2)_4]$, and $\text{cis-}[\text{Ru}(\text{NO})(\text{NH}_3)_2(\text{NO}_2)_2\text{OH}]$ exhibit only photoinduced NO isomers [6,23,24,25]. Even in the case when the GS contains already the nitro and nitrito form NO_2 and ONO , only PLI of the ligand NO could be induced in $\text{PyH}[\text{Ru}(\text{NO})(\text{NO}_2)_2(\text{ONO})\text{py}(\text{OH})]$ and $\text{OC-6-34-}[\text{RuNO}(\text{NO}_2)(\text{ONO})\text{py}_2(\text{OH})]$ [26].

Further interesting effects occur upon heating after irradiation at low temperature. The two PLI obtained by red and blue light irradiation at 10 K decay through intermediate states, which have the same infrared signature. The same state can be generated when irradiating with blue or red light at 100 K, and might correspond to a further isomeric configuration, possibly a chelating (N,O) configuration of one of the NO_2^- . This behaviour leads us to the following hypothesis, summarized in Figure 11: the change of the electronic structure during the relaxation of the PLI as well as possible interactions between the neighbouring NO and NO_2^- ligands result in the adoption of a third PLI, stable in the region of 100-240K. This peculiar behaviour allows to generate different PLI by choosing temperature and irradiation wavelength.

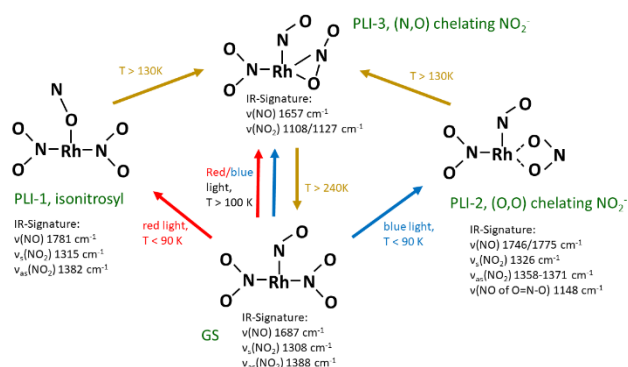


Figure 11: Summary of generation conditions of the various PLI in $[\text{Rh}(\text{NO})(\text{NO}_2)_2(\text{Bu}^t_2\text{PH})_2]$ as a function of temperature and irradiation wavelength. The structures of PLI-1 and PLI-2 are confirmed by photocrystallography, while the structure of PLI-3 is a hypothesis based on infrared spectroscopic results.

Conclusions

Using a combination of photocrystallography and infrared spectroscopy we have shown that in $[\text{Rh}(\text{NO})(\text{NO}_2)_2(\text{Bu}^t_2\text{PH})_2]$ two types of PLI can be induced depending on the selected irradiation wavelength. Using red light, the NO ligand undergoes isomerisation, most probably forming an isonitrosyl configuration. When using blue light, the NO_2^- ligand forms the (O,O')-chelating isomer. Upon heating, these PLI relax back to the GS via an intermediate state.

Conflicts of interest

There are no conflicts to declare.

Acknowledgements

Measurement time on the X-ray diffraction platform of the Institut Jean Barriol is gratefully acknowledged. Financial supports from the French PIA project "Lorraine Université d'Excellence", reference ANR-15-IDEX-04-LUE, and the CPER are acknowledged

References

- M. D. Carducci, M. R. Pressprich and P. Coppens, *J. Am. Chem. Soc.*, 1997, **119**, 2669.
- P. Coppens, I. Novozhilova and A. Kovalevski, *Chem. Rev.*, 2002, **102**, 861.
- D. Schaniel, J. Schefer, T. Woike and V. Petricek, *Phys. Rev. B*, 2005, **71**, 174112; D. Schaniel, J. Schefer, T. Woike, V. Petricek, K. Krämer and H. U. Güdel, *Phys. Rev. B*, 2006, **73**, 174108.
- B. Cormary, I. Malfant, M. Buron-Le-Cointe, L. Toupet, B. Delley, D. Schaniel, N. Mockus, T. Woike, K. Fejfarova, V. Petricek and M. Dusek, *Acta Cryst. B*, 2009, **65**, 612.
- N. Casaretto, S. Pillet, E.-E. Bendeif, D. Schaniel, A. K. E. Gallien, P. Klüfers and T. Woike, *IUCr*, 2015, **2**, 35.
- G. A. Kostin, A. O. Borodin, A. A. Mikhailov, N. V. Kuratieva, B. A. Kolesov, D. P. Pishchur, T. Woike and D. Schaniel, *Eur. J. Inorg. Chem.*, 2015, **29**, 4905; G. A. Kostin, A. A. Mikhailov, N. V. Kuratieva, D. P. Pishchur, D. O. Zharkov and I. R. Grin, *New. J. Chem.*, 2017, **41**, 7758.
- J. S. Garcia, F. Alary, M. Boggio-Pasqua, I. M. Dixon and J. L. Heully, *J. Mol. Model.*, 2016, **22**, 284.
- J. H. Enemark, R. D. Feltham, *Coord. Chem. Rev.*, 1974, **13**, 339.
- M. E. Chacon Villalba, J. A. Guida, E. L. Varetto and P. J. Aymonino, *Spectrochim. Acta A*, 2001, **57**, 367; M. E. Chacon Villalba, J. A. Guida, E. L. Varetto and P. J. Aymonino, *Inorg. Chem.*, 2003, **42**, 2622.
- D. Schaniel, T. Woike, B. Delley, D. Biner, K. W. Krämer and H. U. Güdel, *Phys. Chem. Chem. Phys.*, 2007, **9**, 5149; D. Schaniel, T. Woike, N.-R. Behrnd, J. Hauser, K. W. Krämer, T. Todorova and B. Delley, *Inorg. Chem.*, 2009, **48**, 11399.
- N. Casaretto, B. Fournier, S. Pillet, E.-E. Bendeif, D. Schaniel, A. K. E. Gallien, P. Klüfers and T. Woike, *CrystEngComm*, 2016, **18**, 7260.
- S. K. Brayshaw, T. L. Easun, M. W. George, A. M. E. Griffin, A. L. Johnson, P. R. Raithby, T. L. Savarese, S. Schiffrs, J. E. Warren, M. R. Warren and S. J. Teat, *Dalton Trans.*, 2012, **41**, 90.

- 13 M. R. Warren, S. K. Brayshaw, A. L. Johnson, S. Schiffers, P. R. Raithby, T. L. Easun, M. W. George, J. E. Warren, and S. J. Teat, *Angew. Chem.*, 2009, **121**, 5821.
- 14 A. Y. Kovalevsky, G. King, K. A. Bagley and P. Coppens, *Chem. Eur. J.*, 2005, **11**, 7254.
- 15 H.-C. Böttcher and K. Mereiter, *Inorg. Chem. Commun.*, 2004, **7**, 1225.
- 16 Rigaku Oxford Diffraction. (2017) CrysAlis CCD and CrysAlis RED (Versions 1.171.38.46), Rigaku Oxford Diffraction. Yarnton, England.
- 17 G. M. Sheldrick, *Acta Cryst. A*, 2008, **64**, 112.
- 18 D. Schaniel, N. Mockus, T. Woike, A. Klein, D. Sheptyakov, T. Todorova and B. Delley, *Phys. Chem. Chem. Phys.*, 2010, **12**, 6171; M. A. Hitchman and G. L. Rowbottom, *Coord. Chem. Rev.*, **1982**, **42**, 55.
- 19 A. M. Heyns and D. de Wall, *Spectrochim. Acta A*, **1989**, **45**, 905.
- 20 S. Dominguez, P. Albores and F. Fagalde, *Polyhedron*, 2014, **67**, 471.
- 21 I. Roger, C. Wilson, H. M. Senn, S. Sproules and M. D. Symes, *R. Soc. open sci.*, **2017**, **4**, 170593.
- 22 I. R. Laskar, D. Das, G. Mostafa, T.-H. Lu, T.-C. Keng, J.-C. Wang, A. Ghosh and N. R. Chaudhuri, *New. J. Chem.*, **2001**, **25**, 764.
- 23 D. V. Fomitchev and P. Coppens, *Inorg. Chem.*, **1996**, **35**, 7021.
- 24 A. Puig-Molina, H. Müller, A.-M. Le Quéré, G. Vaughan, H. Graafsma and A. Kvik, *Z. Anorg. Allg. Chem.*, **2000**, **626**, 2379.
- 25 V. Vorobyev, G. A. Kostin, N. V. Kuratieva and V. A. Emelyanov, *Inorg. Chem.*, **2016**, **55**, 9158.
- 26 G. A. Kostin, A. A. Mikhailov, N. V. Kuratieva, S. V. Tkachev, D. Schaniel and T. Woike, *Eur. J. Inorg. Chem.*, 2016, **25**, 4045.

Supplementary Material

Wavelength-selective photoisomerisation of nitric oxide and nitrite in a rhodium complex

D. Schaniel, E.-E. Bendeif, T. Woike, H.-C. Böttcher, and S. Pillet

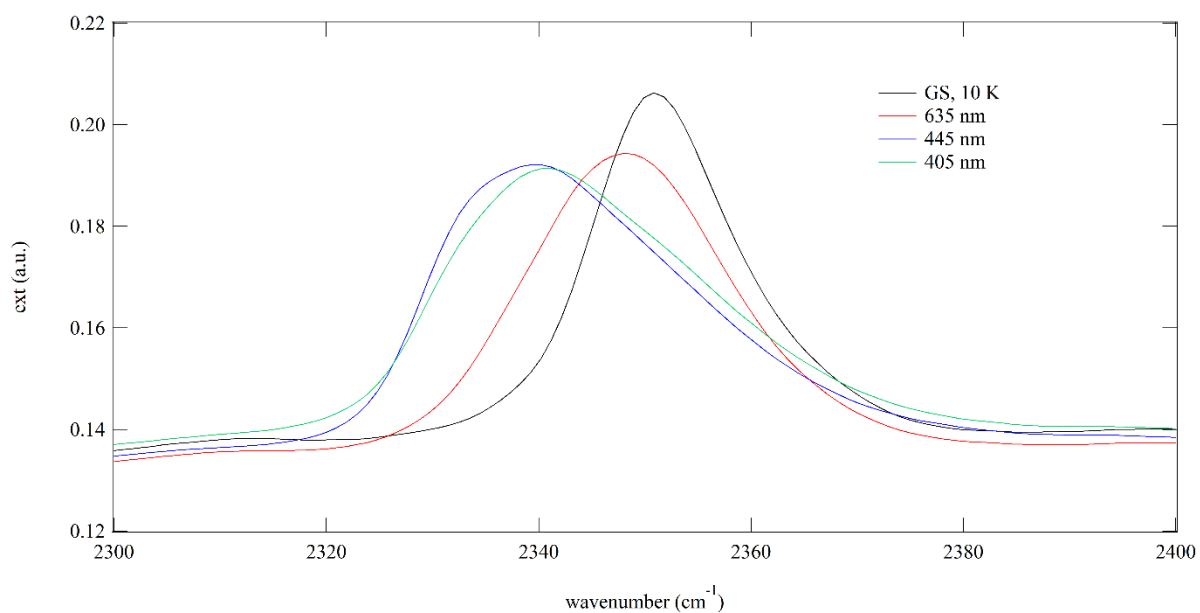


Fig. S1: Infrared spectra as a function of irradiation wavelength in the spectral range of the PH vibrational bands.

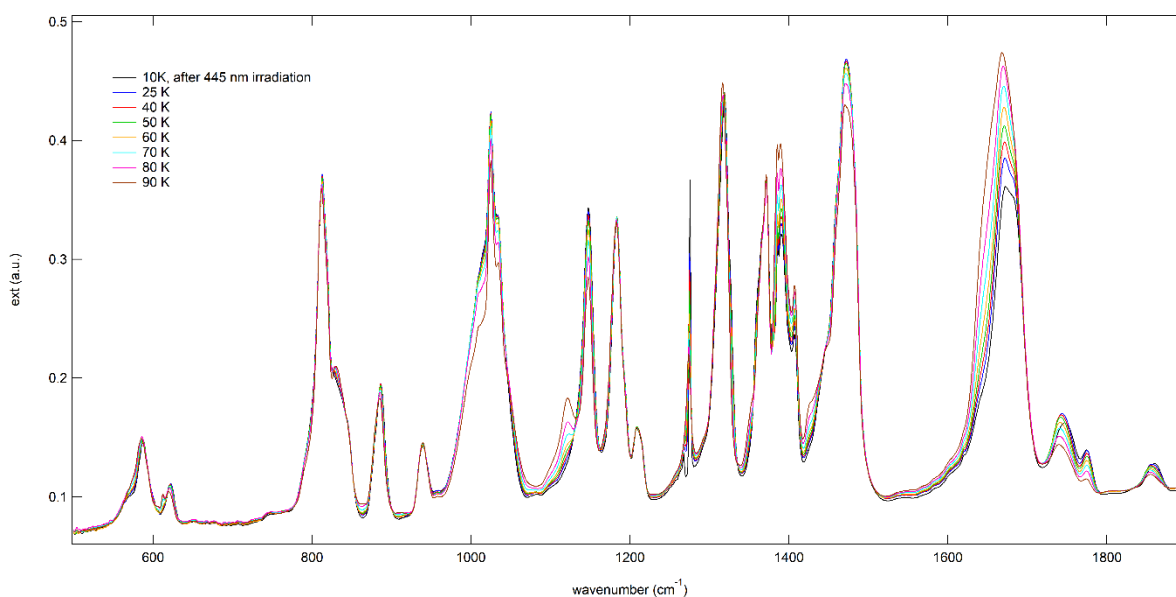


Fig. S2: Infrared spectra upon heating after irradiation at 10 K with 445 nm: 10 - 90 K.

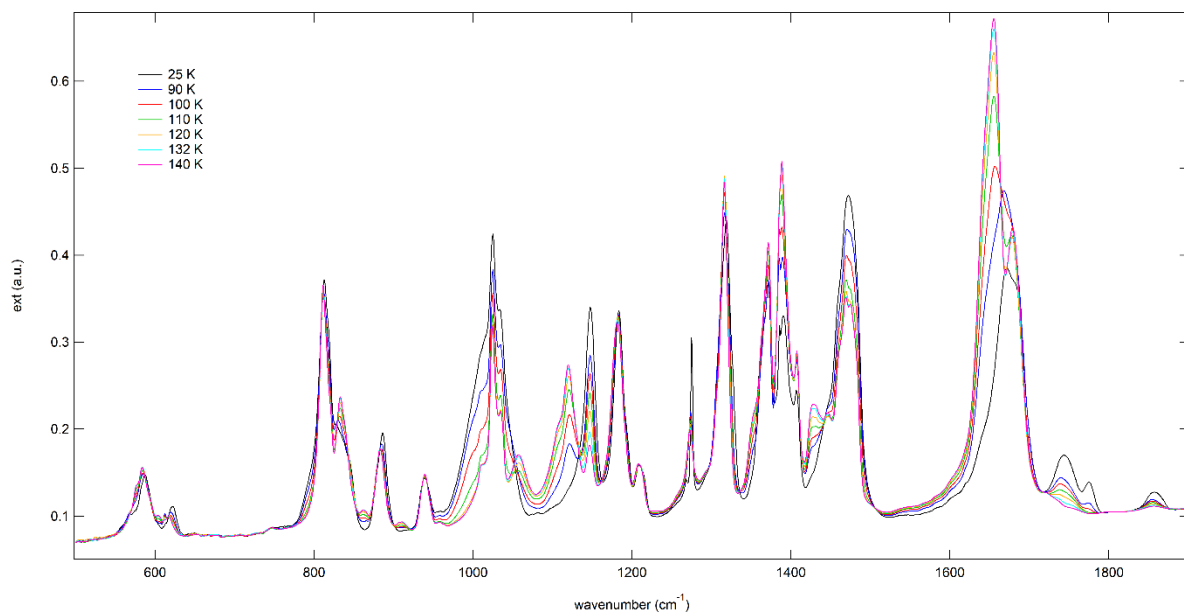


Fig. S3: Infrared spectra upon heating after irradiation at 10 K with 445 nm: up to 140 K.

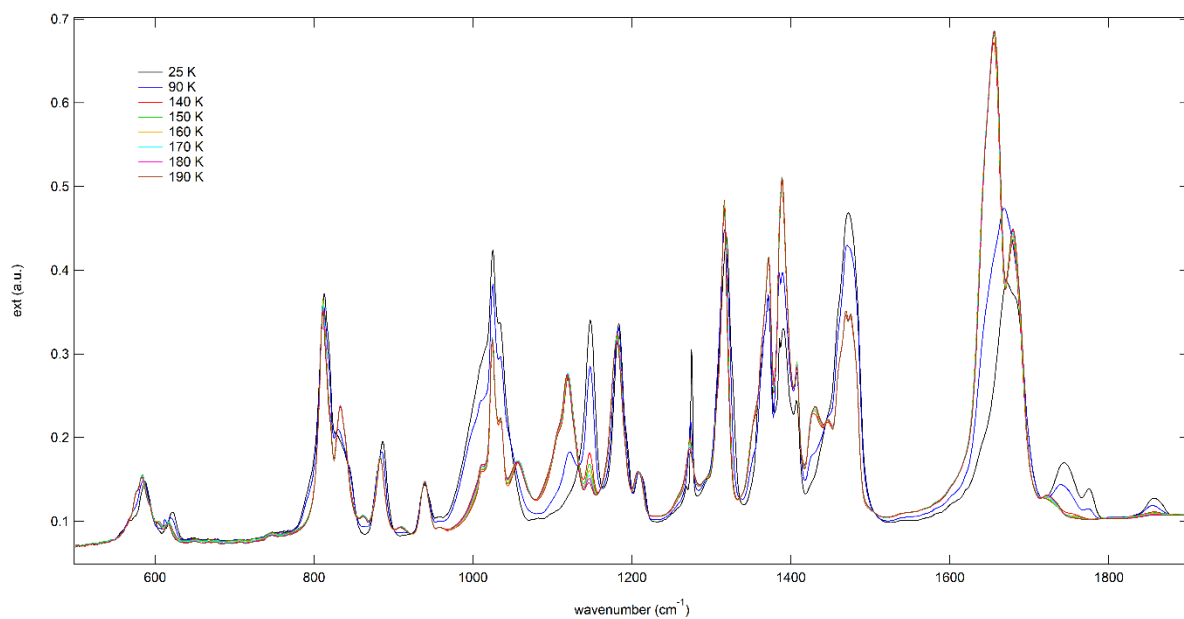


Fig. S4: Infrared spectra upon heating after irradiation at 10 K with 445 nm: up to 190 K.

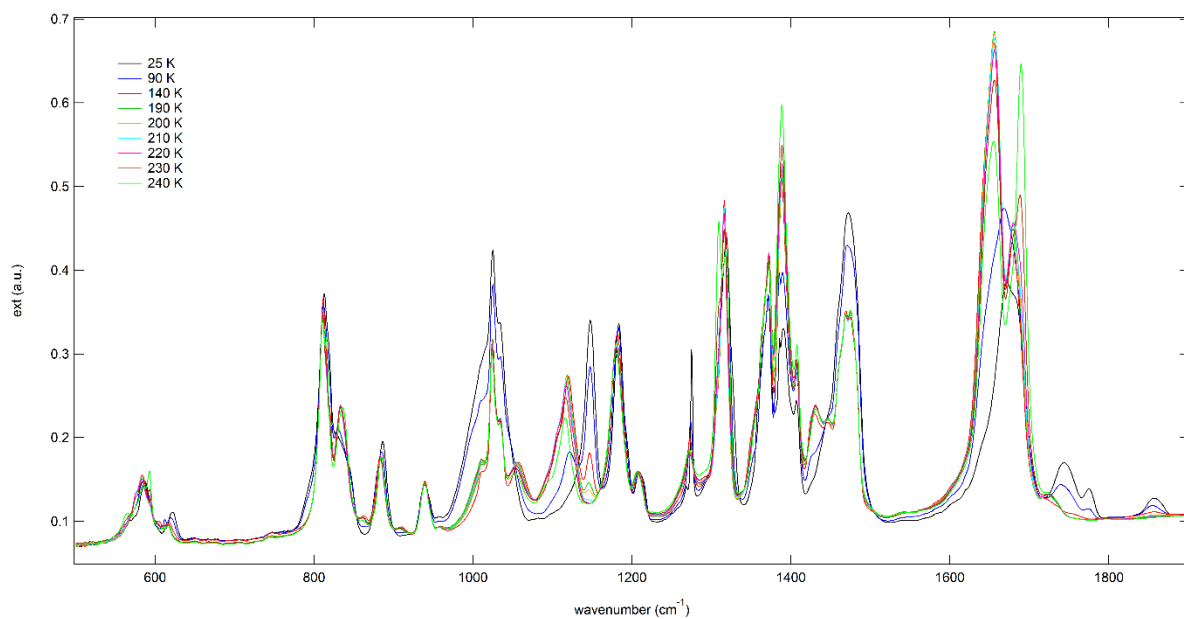


Fig. S5: Infrared spectra upon heating after irradiation at 10 K with 445 nm: up to 240 K.

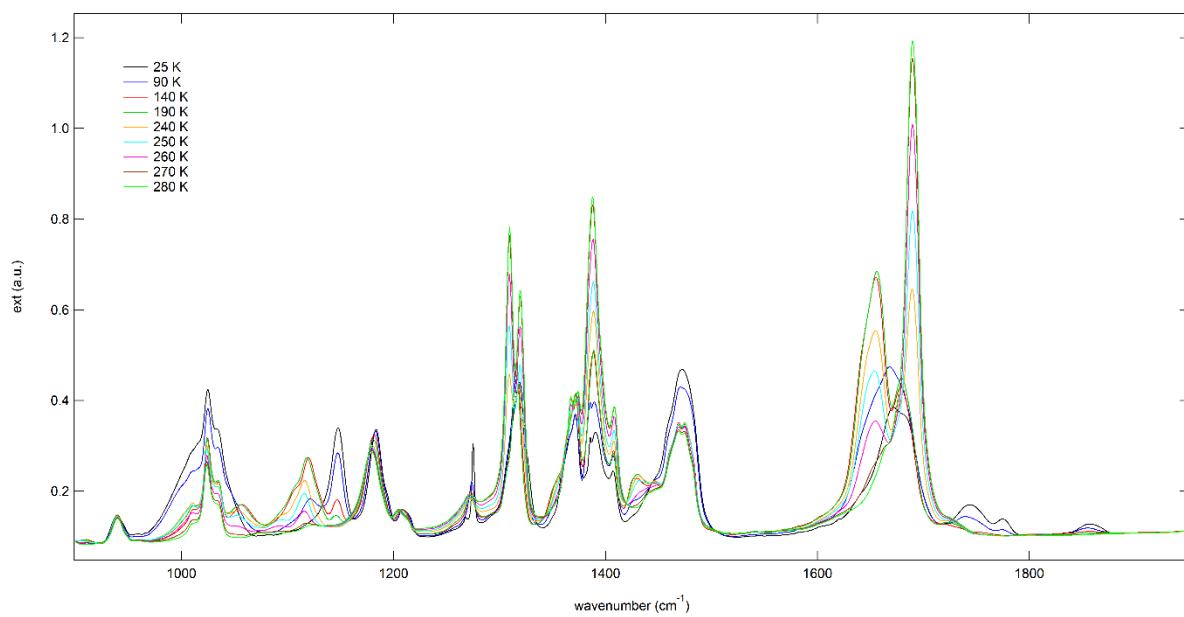


Fig. S6: Infrared spectra upon heating after irradiation at 10 K with 445 nm: up to 280 K.

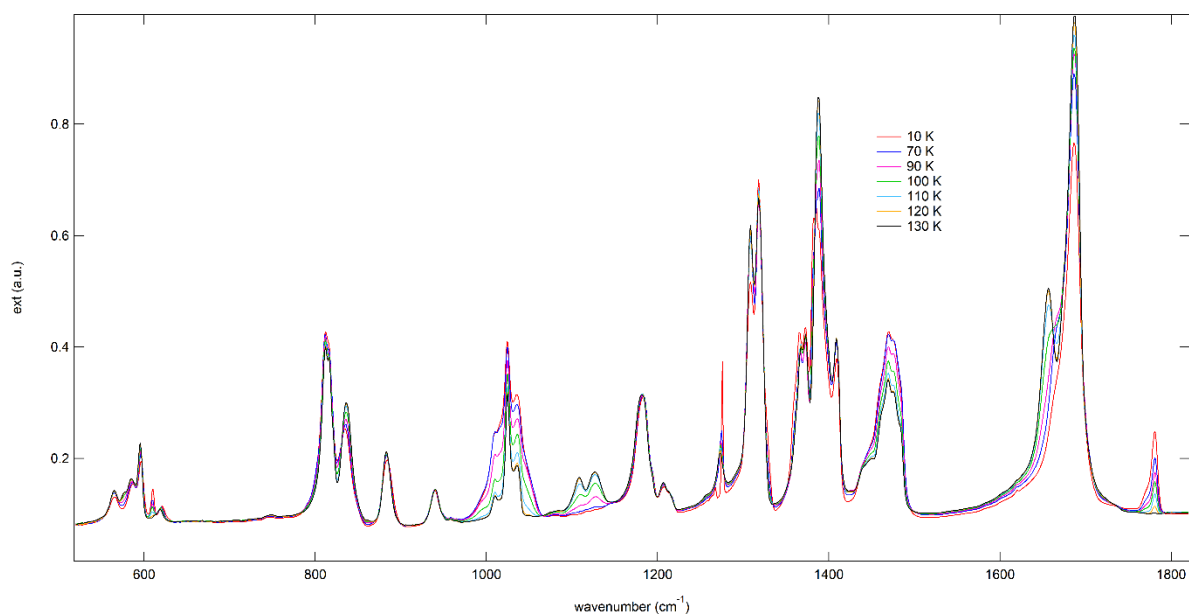


Fig. S7: Infrared spectra upon heating after irradiation at 10 K with 635 nm: 10 – 130 K.

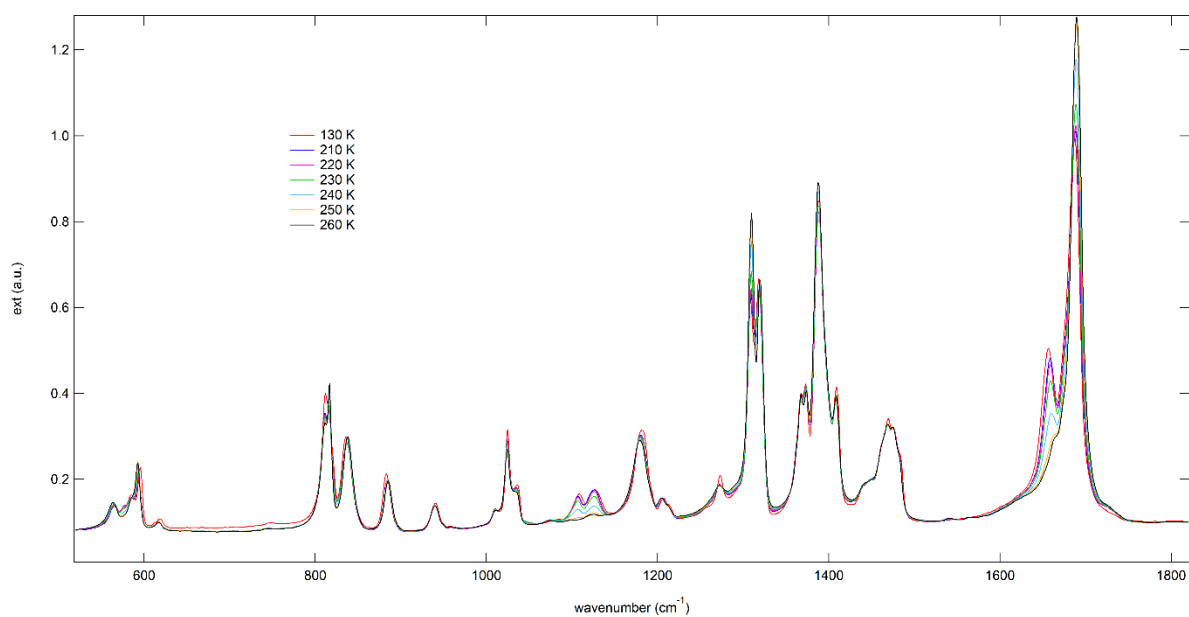


Fig. S8: Infrared spectra upon heating after irradiation at 10 K with 635 nm: 130 – 260 K.

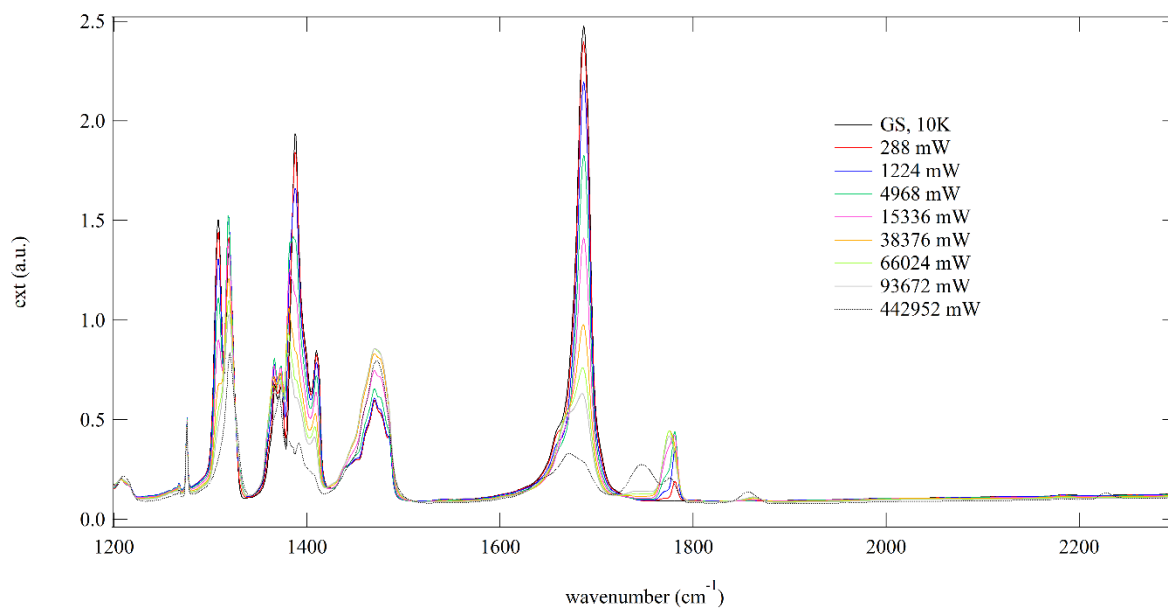


Fig. S9: Infrared spectra as a function of irradiation fluence at 10 K with 445 nm. Beyond about 200 mJ/cm^2 the signature of free NO in KBr at 2220 cm^{-1} becomes visible.